

Received October 16, 2020, accepted October 19, 2020, date of publication October 22, 2020, date of current version November 5, 2020.

Digital Object Identifier 10.1109/ACCESS.2020.3033148

Motion Kinematics Analysis of a Horse Inspired Terrain-Adaptive Unmanned Vehicle With Four Hydraulic Swing Arms

XUANYI ZHOU¹ , (Graduate Student Member, IEEE), JILIN HE¹,
QINGHUA HE¹, CHANGJI REN¹, BHUSHAN², AND MIAOLEI HE³ , (Member, IEEE)

¹State Key Laboratory of High Performance Complex Manufacturing, Central South University, Changsha 410083, China

²Control Engineering at DIAG, Sapienza University of Rome, 00185 Rome, Italy

³College of Engineering and Design, Hunan Normal University, Changsha 410083, China

Corresponding author: Jilin He (hejilin@csu.edu.cn)

This work was supported in part by the Changsha Science and Technology Project under Grant kq2004081, and in part by the Chinese Scholarship Council 201906370138.

ABSTRACT All terrain vehicles (ATV) perform tasks in unstructured environments where the advanced adaptive ability of rigid terrain has become a key factor. In this article, we propose a novel horse inspired all terrain eight-wheeled vehicle with four swing arms for transportation in the mountain battlefield. The mechanism structure and system configuration of the ATV are designed based on the horse leg kinematics analysis. In order to analyze the obstacle surmounting strategy of the ATV, the kinematics model and the center of gravity of the ATV are represented. A model reference adaptive control method is proposed for the hydraulic attitude control system. Then the model for obstacle surmounting is proposed for dynamics performance and geometric kinematics. Additionally, the simulation is executed in Adams to verify the analysis and strategy. Finally, the experiment is demonstrated for climbing a vertical wall, which is a challenging and typical terrain of the mountain battlefield.


INDEX TERMS All terrain vehicle, obstacle surmounting, motion kinematics analysis.

I. INTRODUCTION

Unmanned Ground Vehicles (UGV) are widely applied in hazardous environments where human activities are restricted such as nuclear rescue [1], field reconnaissance [2] and unmanned combat [3]. In order to expand the scope of the UGV, varieties of ATV are proposed with strong ability of environmental adaptation in both military and civil applications [4]. A Squad Mission Support System (SMSS) with 6×6 wheels is developed by Lockheed-Martin Corporation [5]. The SMSS can cross obstacles up to 0.41m due to its superior dynamics. However, wheeled ATV such as SMSS has weak ability to absorb high frequency vibration without ground clearance adjustment ability of the active suspension [6]. A four-track ATV with double swing arms is developed by IRobot Corporation [7]. The swing arms can be applied to climb steps, surmount obstacles and maintain contact with the ground on uneven roads. Although tracked ATV has large

ground contact area leading to excellent terrain adaptability [8], the mechanical transmission system has low energy efficiency [9]. The four legged robot BigDog developed by Boston Dynamics has exceptional rough-terrain mobility with high payload up to 100kg [10]. And the atlas humanoid robot is able to climb steps, jump and carry to replace humans activities in certain special environments to perform tasks with superior and stable control strategy and environmental perception technology [11]. For the legged ATV, it has good adaptability performance on rugged terrain with its discrete mechanism and more degrees of freedom [12]. However, the speed of legged ATV is limited and the frequent impacts of leg and the ground reduce energy efficiency [13]. It is interesting to combine the excellent adaptability and the high speed of legged ATV with good energy efficiency of wheeled ATV.

A novel configuration of the hybrid robot, including a single caster-leg mechanism for the skid steerable wheeled vehicle, is proposed in [14]. The tip-over stability and maneuverability are analyzed while surmounting the maximum height of 140mm. A new leg-wheel robot configuration

The associate editor coordinating the review of this manuscript and approving it for publication was Shihong Ding .



(a) Horse clearing a fence



(b) Obstacle surmounting of the ATV

FIGURE 1. Comparison of obstacle surmounting between horse and ATV.

(TurboQuad) is designed in [15]. The robot is equipped with a novel conversion mechanism that can switch the form of the drive mechanism between the wheels and the legs. In the legged mode, TurboQuad can surmount step obstacle up to 0.145m. Dynamics analyses and simulations of a novel two-wheeled and hopping robot are analyzed in [16]. Due to the expansion of the scope of human resource utilization [17], those lightweight robots with poor load capacity are not able to meet the load capacity requirements in many scenarios, such as disaster relief [18], mining haulage [19] and military transportation [20]. A parallel leg-wheeled robot (NAZA) is introduced in [21] for the applications of heavy payload. With six degrees of freedom parallel legs, NAZA can only negotiate 65cm slope obstacle [22]. The Crusher, developed by the National Robotics Engineering Center of Carnegie Mellon University for the military scenario, is an ATV with six longitudinal independent suspensions in an extensive range of complex, off-road terrains [23]. The Crusher is capable of carrying over 3600 kilograms of payload and armor at high-off road speeds and across extreme terrains negotiating a 2.4 times wheel-radius height wall. The Multifunctional Utility/Logistics and Equipment Vehicle (MULE) with six-swing arms is developed by Lockheed-Martin Corporation [24]. By controlling the six swing arms, the angle of the MULE can be adjusted to change vehicle ground clearance and attitude during the obstacle surmounting. A direct yaw-moment control system applying sliding mode and nonlinear disturbance observer techniques is proposed in [25] to improve vehicle stability in critical scenarios [26]. However, a stable attitude control algorithm is required for the active swing arms of MULE, which reduces the efficiency of the ATV.

With the development of information technology, numerous terrain adaptive methods are proposed. A new passive adaptive control method is presented in [27] for quadruped robots to achieve compliant balance. A novel variable passive-compliant element is designed for quadruped robot control [28]. [29] proposes a new passive independent suspension system for a tracked skid steering robot adaptively in

complex terrain. However, all of the above passive adaptive methods are applied for low load capacity and the control strategy is complex, which can not be implemented in mountain transportation.

Since the self-adaptive ability and the mechanism of the obstacle surmounting are the key factors that restrict the passage of ATV in complex and hazardous environments [30], a novel wheel-legged all terrain vehicle, called “Dragon Horse” is presented in this article.

In order to meet the strong adaptability in complex terrain, the ATV is designed to ensure its all-terrain adaptability in harsh terrain environments such as mountain plateaus, ravines, hills, and river beaches. The drive mode of the ATV is distributed drive based on wheel hydraulic motors, which can provide superior power performance. The climbing mechanism is a wheel-leg configuration, driven by two hydraulic cylinders, which can actively control the stroke and achieve the leveling, pitching, roll and other posture adjustments. The slip steering system is assisted by the small-angle geometric steering mode to improve the flexibility of movement in narrow spaces on the battlefield. The design meets the requirements of high-mobility patrol, combat, and reconnaissance in the complex environment of the battlefield.

The inspiring strategy of the obstacle surmounting is shown in Fig.1. With four-swing horse-like arms, the ATV is able to surmount a vertical obstacle by planning the arms posture and adapt to the terrain. The powerful hydraulic system enables the ATV sufficient power for the scenario. The motion kinematics of the obstacle surmounting are analyzed in the article and the hydraulic model and posture control method are presented to control the posture during the obstacle surmounting. The innovation of this article is shown as below:

- A horse inspired all terrain-adaptive unmanned vehicle is designed to achieve a strong ability of environmental adaptation, especially climbing a vertical wall.
- The obstacle surmounting strategy is proposed by analyzing the motion kinematics of the ATV.

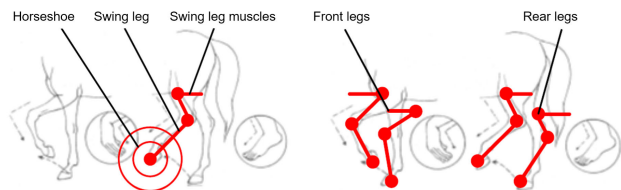


FIGURE 2. Schematic diagram of horse leg kinematics analysis.

- A model reference adaptive control method is proposed to control the hydraulic swing arms system to achieve good performance of the posture for the swing arms.

The remainder of the paper is organized as follows. In section II, the design and structure model of the ATV is presented. In section III the hydraulic attitude control based on MRAC is introduced. In section IV the obstacle surmounting strategy is proposed in details. In section V the simulation and field experiment are introduced to demonstrate the effectiveness of the ATV.

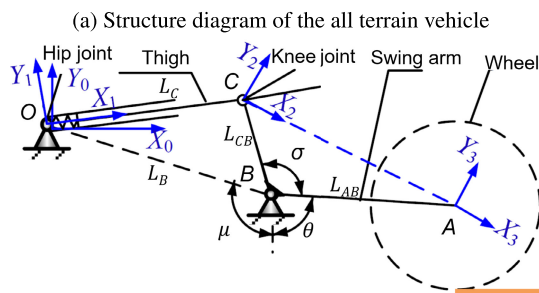
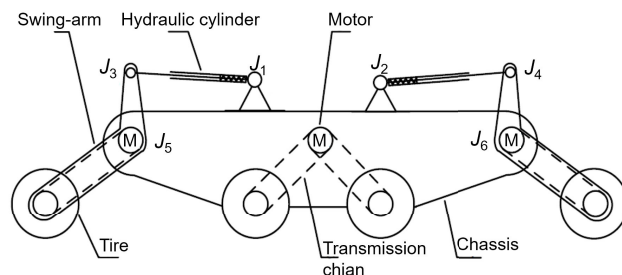
II. DESIGN AND SYSTEM CONFIGURATION OF THE ATV

A. HORSE INSPIRED CONCEPT

Inspired by horse clearing a fence, as shown in Fig.1(a), the structure of the ATV is designed accordingly. Taking the negotiating a fence as an example, the joints of the horse's legs are composed of the horseshoe, swing leg and swing leg muscles, as shown in Fig. 2. The horse legs can be simplified into two parts, the front legs and the rear legs. Driven by the muscle force of the swing leg, the swing leg performs actions such as raising and lowering, and finally drives the horseshoe to perform walking or jumping behaviors. When the horse's nervous system controls the coordinated movement of the front and rear legs, it can pass through the body posture adjustment to achieve obstacle surmounting. According to mechanism design theory, the contact pressure of the low pair is smaller than that of the high pair, and the reliability of the low pair is higher than the high pair. The reliability and maintainability are much better with fewer motion mechanism connections.

Referring to the kinematic principles of the horse's legs shown in Fig.3(b), O denotes the hip joint, which connects the swing arm and the chassis, C denotes the knee joint, which connects the swing arm and the hydraulic cylinder, and B is the fixed support hinge point of the swing arms and ATV body. A is the end joint of the leg, which is the center position of the wheel. OC denotes the hydraulic cylinder, while CBA denotes the swing arm. The posture of the ATV is controlled by varying the stroke of the hydraulic cylinder. When the hydraulic cylinder elongates or retracts, C is changing accordingly, and the swing arms rotate around B . With the rotational ability to adjust the contact state of the tire and the ground, the ATV can maintain stability through transportation applications.

The horizontal and vertical slope leveling of the vehicle body are realized by swinging the left and right swing arms or the front and rear swing arms in opposite directions,



(b) The arm geometry model

FIGURE 3. Structure of the ATV.

as shown in Fig.4. The climbing performance of the ATV is presented in Table.1. According to the displacement amplitude design parameters of the ATV swing arm mechanism, the maximum vertical slope leveling angle is 10° , and the maximum horizontal slope leveling angle is 8° . At the same time, the swing arms can attenuate high-frequency ground vibrations in high-speed driving. In the obstacle surmounting, the swing arms is operated actively to ensure the effective contact between the vehicle and the obstacle, which is a necessary condition for providing sufficient driving force. The hydraulic cylinder can change the stroke to drive the thigh to elongate or retract. During the operating process, the swing arms can rotate around B . With the rotational ability, the ATV is able to keep stability during transportation in the mountains. The climbing performance of the ATV is presented in Table.1.

On the basis of studying the biological characteristics and mechanism of horse clearing a fence, this article adopts a simple three-link motion plane obstacle crossing mechanism, as shown in Fig. 3(b), which includes hydraulic cylinders as swing leg muscles, swing arm as swing leg and the wheel as a horseshoe.

The structure diagram of the ATV with multiple swing arm is shown in Fig.3(a). It is composed of the chassis system, the swing arm system, hydraulic cylinder device, hydraulic wheel-drive system. 8×6 full hydraulically-driven chassis is applied. Four swing arms hydraulic motors are located around the hinge point J_5 and J_6 to rotate the swing arms through gear chain transmission. Two main body hydraulic motors are located in the middle of the body, and the one-sided motor drives two wheels in the middle to rotate at the same time through the gear chain transmission. The hydraulically

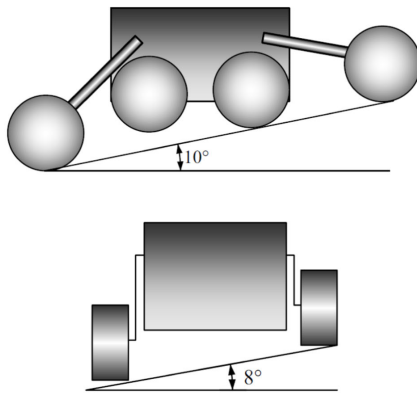


FIGURE 4. Leveling in the vertical and horizontal terrain.

TABLE 1. The climbing performance of the ATV.

maximum gradeability	Maximum longitudinal leveling angle	Maximum horizontal leveling angle
62.5%	10°	8°

TABLE 2. The DH parameters of the swinging arms.

j	α_{j-1}	a_{j-1}	d_j	θ_j
1	0	0	0	$90^\circ + \angle AOB - \mu$
2	0	L_C	0	$180^\circ - \angle ABW - \angle OBA$
3	0	v	0	0

driven swing arm and chassis system have higher maneuverability than the electric drive system, which can realize stepless speed regulation and high torque. It is designed for high-frequency shock and vibration environments when obstacle surmounting in complex terrains.

Applying O as the fixed base of the swing arm, the Denavit-Hartenberg method is used to establish the coordinate system of the swing arm. The DH parameters of the swinging arm are shown in Table.2. The degree of freedom (DOF) of the swing arm D can be expressed as:

$$D = f(n - \hat{j} - 1) + \sum_{i=1}^g d_i - \lambda \quad (1)$$

where n denotes the connection number; \hat{j} denotes the joints number; d_i denotes the DOF at i th joint, and λ is the local DOF number. For the structure of the ATV, $f = 3$. The degree of freedom of the swing arm can be obtained as $D = 2$. When the swing arms are controlled by the planning method, the wheels of the ATV can contact the ground during obstacle surmounting.

where $v = \sqrt{L_{CB}^2 + L_{AB}^2 - 2L_{CB}L_{AB} \cos \sigma}$. According to the robotic theory, the rotation transformation matrix can be expressed as:

$${}^W_O T = {}^B_O T {}^W_B T \quad (2)$$

$$\begin{cases} {}^O_B T = \text{Trans}(L_C, 0, 0) \text{Rot}(z, 90^\circ + \angle AOB - \mu) \\ {}^B_W T = \text{Trans}\left(\sqrt{L_{CB}^2 + L_{AB}^2 - 2L_{CB}L_{AB} \cos \sigma}, 0, 0\right) \end{cases} \quad (3)$$

From the triangle theorem, the relationship of each angle and the rod can be obtained as:

$$\cos \angle OBC = \cos(\mu + \sigma + \theta) = \frac{L_{CB}^2 + L_A^2 - L_C^2}{2L_{CB}L_A} \quad (4)$$

$$\frac{L_C}{\sin \angle OBC} = \frac{L_A}{\sin \angle OCB} = \frac{L_{CB}}{\sin \angle BOC} \quad (5)$$

$$\frac{L_{AB}}{\sin \angle BCA} = \frac{\sqrt{L_{CB}^2 + L_{AB}^2 - 2L_{CB}L_{AB} \cos \sigma}}{\sin \sigma} \quad (6)$$

Combing Eq.2 with Eq.6, the coordinates of the wheel center (x_A, y_A) can be expressed as:

$$\begin{cases} x_A = L_{AB} \sin \theta + L_A \sin \mu \\ y_A = L_{AB} \cos \theta - L_A \cos \mu \end{cases} \quad (7)$$

And the relationship of the swing angle θ and hydraulic cylinder stroke L_C is defined as:

$$\theta = \arccos\left(\frac{L_{CB}^2 + L_A^2 - L_C^2}{2L_{CB}L_A}\right) - \mu - \sigma \quad (8)$$

where μ and σ are shown in Fig.3(b). And the coordinate system is built as in Fig.3(b). The functions of the wheel center coordinate can be obtained as:

$$\begin{cases} x_W = L_{AB} \sin \theta + L_A \sin \mu \\ y_W = L_{AB} \cos \theta - L_A \cos \mu \end{cases} \quad (9)$$

where L_{AB} denotes the length of the swing arm, $L_{AB} = 705\text{mm}$, $L_{CB} = 420\text{mm}$, $L_A = 1400\text{mm}$, $\mu = 108^\circ$, $\sigma = 115^\circ$, and $\theta = [30^\circ \ 110^\circ]$.

B. KINEMATIC MODEL OF THE ALL TERRAIN VEHICLE

The transform swing arms of the ATV are applied to surmount obstacles. The kinematic model for the wheel center and the hydraulic cylinder stroke is established, which is used as both theoretical principles for the robot vehicle design and guidance of the motion strategy design. The relationship between the wheel center velocity and the arm angular rate is defined as:

$$\begin{cases} \dot{s} = J(\theta) \cdot \dot{\theta} \\ s = \begin{bmatrix} x & y \end{bmatrix}^T \end{cases} \quad (10)$$

where $J(\theta)$ denotes the Jacobian matrix of the swing arm. Combining with Eq.10, the result is obtained as:

$$J(\theta) = L_{AB}[\cos \theta \quad -\sin \theta]^T \quad (11)$$

The swing arm angular rate can be expressed as:

$$\dot{\theta} = J(L_C) \dot{L}_C \quad (12)$$

where the $J(L_C)$ denotes the Jacobian matrix of the hydraulic cylinder. Substituting Eq.8 into Eq.12, we can obtain:

$$J(L_C) = \frac{L_C}{L_{CB}L_A} \left[1 - \left(\frac{L_{CB}^2 + L_A^2 - L_C^2}{2L_{CB}L_A} \right)^2 \right]^{-\frac{1}{2}} \quad (13)$$

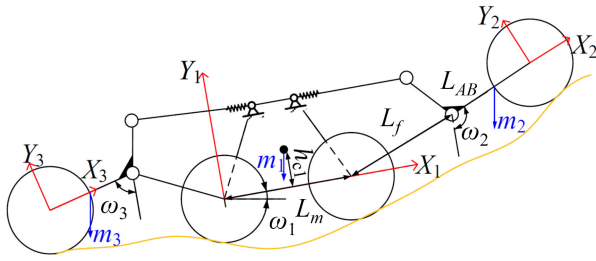


FIGURE 5. Coordinate system of the all terrain vehicle.

Combining Eq.10 to 13, the kinematic model of swing arms can be obtained as:

$$\begin{cases} x = \int \frac{L_{AB}L_C}{L_{CB}L_A} \left[1 - \left(\frac{L_{CB}^2 + L_A^2 - L_C^2}{2L_{CB}L_A} \right)^2 \right]^{-\frac{1}{2}} \cos \theta dL_C \\ y = - \int \frac{L_{AB}L_C}{L_{CB}L_A} \left[1 - \left(\frac{L_{CB}^2 + L_A^2 - L_C^2}{2L_{CB}L_A} \right)^2 \right]^{-\frac{1}{2}} \sin \theta dL_C \end{cases} \quad (14)$$

C. GRAVITY CENTER ANALYSIS

The center of gravity of the ATV is a crucial factor in determining whether the vehicle can surmount the obstacle or not. Considering the posture of the ATV, the coordinate system of each subsystem is established, as shown in Fig.5. The coordinate transformation matrix 0T_1 of the coordinate system $X_1O_1Y_1$ of the ATV to the world coordinate system $X_0O_0Y_0$ is obtained as:

$${}^0T_1 = \text{Trans}(d_x, d_y, d_z) \text{Rot}(z, \theta) \text{Rot}(y, \eta) \text{Rot}(x, \delta) \quad (15)$$

where d_x, d_y, d_z are the displacement of the ATV in x, y, z directions. θ, δ, η are the pitch, roll, yaw angle of the ATV, respectively. The transformation matrixes of the front swing arm (1T_2) and the rear swing arm (1T_3) coordinate system are obtained as:

$$\begin{aligned} {}^1T_2 &= \begin{pmatrix} c_2 & -s_2 & 0 & L_m + L_f \cos \epsilon + L_{AB}s_2 \\ s_2 & c_2 & 0 & L_f \sin \epsilon - L_{AB}c_2 \\ 0 & 0 & 1 & 0 \\ 0 & 0 & 0 & 1 \end{pmatrix} \\ {}^1T_3 &= \begin{pmatrix} c_2 & -s_2 & 0 & -L_f \cos \epsilon - L_{AB}c_3 \\ s_2 & c_2 & 0 & L_f \sin \epsilon - L_{AB}s_3 \\ 0 & 0 & 1 & 0 \\ 0 & 0 & 0 & 1 \end{pmatrix} \end{aligned} \quad (16)$$

where c_i and s_i represent $\cos \omega_i$ and $\sin \omega_i$ ($i=2, 3$), respectively. And the coordinate system $X_1O_1Y_1$ of ATV is defined as

$${}^1C = \frac{\sum_{i=1}^3 {}^1T_i^i C_i m_i}{M} \quad (17)$$

where M represents the total mass of the ATV, and iC_i represents the coordinate matrix of the ATV's main body, front

swing arm and rear swing arm in their respective coordinate systems defined as:

$$\begin{cases} {}^1C_1 = \begin{pmatrix} \frac{L_m}{2} & h_{c1} & 0 & 1 \end{pmatrix}^T \\ {}^2C_2 = \begin{pmatrix} -\frac{L_{AB}}{2} & 0 & 0 & 1 \end{pmatrix}^T \\ {}^3C_3 = \begin{pmatrix} \frac{L_{AB}}{2} & 0 & 0 & 1 \end{pmatrix}^T \end{cases} \quad (18)$$

Assuming that the ATV will not yaw and slip during the obstacle surmounting, the yaw and roll angles are all zero. Combining Eq.15 with Eq.18, the coordinate of the ATV in the world coordinate system is obtained as:

$${}^0C = {}^0T_1 {}^1C = \begin{pmatrix} \frac{Ac_1 - Bs_1}{As_1 + Bc_1} + d_x \\ \frac{M}{M} + d_y \\ d_z \\ 1 \end{pmatrix} \quad (19)$$

where $A = \frac{L_m}{2}m_1 + [L_{AB}(s_2 - \frac{c_2}{2}) + L_m]m_2 + [L_{AB}(\frac{c_2}{2} - c_3) - L_f \cos \epsilon]m_3$, and $B = h_{c1}m_1 + [L_{AB}(-c_2 - \frac{s_2}{2}) + L_f \sin \epsilon]m_2 + [L_{AB}(\frac{s_2}{2} - s_3) + L_f \sin \epsilon]m_3$.

III. HYDRAULIC ATTITUDE CONTROL BASED ON MRAC

A. MODEL OF THE HYDRAULIC SYSTEM

To implement attitude control during the obstacle surmounting, the dynamic model of the hydraulic cylinder is introduced with the dynamics of the hydraulic system, composed of four electro-hydraulic valves and one hydraulic pump. In the swing arm attitude control system, the engine provides the power source for the hydraulic pump B, and the hydraulic pump provides the drive for the swing arm hydraulic cylinder to realize the swing of the swing arm and the adjustment of the vehicle attitude. The transfer function between the displacement of the electro-hydraulic valve spool and the control current is presented as

$$P_v(s)/I_e(s) = K_v/(1 + bTs) \quad (20)$$

where K_i is the current gain of the electro-hydraulic valve, and b denotes the time constant of inertia. $I_e = I(t) - i_i$ is the effective input current of the electro-hydraulic valve, $I(t)$ denotes the control current of the electro-hydraulic valve, and i_i is the initial current to eliminate the dead zone.

The flowrates in chamber 1 and chamber 2 of the electro-hydraulic valve, are defined as Q_1 and Q_2 , respectively:

$$\begin{aligned} Q_1 &= \begin{cases} C_f A_g P_v \sqrt{2\Delta P / \rho d} & I_t \geq 0 \\ C_f A_g P_v \sqrt{2(P_{c1} - p_r) / \rho d} & I_t < 0 \end{cases} \\ Q_2 &= \begin{cases} C_f A_g P_v \sqrt{2(P_{c2} - p_r) / \rho d} & I_t \geq 0 \\ C_f A_g P_v \sqrt{2\Delta P / \rho d} & I_t < 0 \end{cases} \end{aligned} \quad (21)$$

where C_f is the discharge coefficient, A_g and P_v denote the area gradient and the spool position of the electro-hydraulic

valve, ρ_d denotes the density of the hydraulic oil, P_{c1} , P_{c2} are the pressures at chamber 1 and chamber 2 of the electro-hydraulic valve, respectively, ΔP denotes the pressure threshold for the relief valve, p_{sp} is the supplied pressure of the output pump, p_r presents the return pressure of the oil return to the tank. The definition of Q_1 can be simplified as:

$$Q_1 = K_f X_v(t), \quad I(t) \geq 0 \quad (22)$$

where K_f denotes the flow gain coefficient of the electro-hydraulic valve and is defined as $K_q = C_d W K \sqrt{2\Delta P/\rho}$. With the development of sealing technology, leakage can be ignored in operation. Moreover, the continuous equation of the hydraulic cylinder is defined as:

$$\begin{aligned} Q_1 &= S_1 \dot{y}_p + V_1 \cdot \dot{P}_{c1}/\beta_e \\ Q_2 &= S_2 \dot{y}_p - V_2 \cdot \dot{P}_{c2}/\beta_e \end{aligned} \quad (23)$$

where S_1 and S_2 denote the effective piston area of the chamber 1 and chamber 2, respectively, V_1 and V_2 are volumes of the in and out hydraulic cylinder, respectively, y_p is the displacement of the piston, β_e denotes the bulk modulus. The hydraulic drive force can be defined as:

$$F_H = p_{c1}S_1 - p_{c2}S_2 = M_p \dot{y}_p + B_p \dot{y}_p + F_l \quad (24)$$

where F_H is the hydraulic driving force, B_p denotes the damping coefficient of the piston and the load, F_l is the load force, which is opposite to the direction of movement of the piston, M_p is the quality of the piston. To further simplify the model, assume:

$$Q_1/Q_2 = S_1/S_2 \quad (25)$$

Substituting Eq.22 into Eq.23, we can obtain:

$$\begin{aligned} K_f P_v(t) &= S_1 \dot{y}_p + V_{c1} \cdot \dot{P}_{c1}/\beta_e \\ \frac{S_2}{S_1} K_f P_v(t) &= S_2 \dot{y}_p - V_2 \cdot \dot{P}_{c2}/\beta_e \end{aligned} \quad (26)$$

The dynamic mode of the hydraulic system can be presented by combining the results of the Laplace transformation of Eq.26 and Eq.24:

$$Y(s) = [b_v P_v(s) + b_s F_l(s)]/s(a_s s^2 + a_b s + a_c) \quad (27)$$

where $b_v = \beta_e K_f (S_1 V_2 + V_1 S_2^2/S_1)$, $b_s = -V_1 V_2$, $a_0 = V_1 V_2 M_p$, $a_1 = B_p V_1 V_2$, $a_2 = \beta_e (V_2 S_1^2 + V_1 S_2^2)$

B. MODEL REFERENCE ADAPTIVE CONTROL

From the experiments of the hydraulic cylinder, the response process shows that the system can approximately be simplified as a first-order system by combining Eq.20 and Eq.27:

$$Y(s) = K_f K_v I_e(s)/s S_1 (1 + b_T s) \quad (28)$$

The relation of the velocity of the hydraulic cylinder $v_p(s)$ and control current can be defined as:

$$v(s) = K_f K_v I(s)/A_1 (1 + b_s) \quad (29)$$

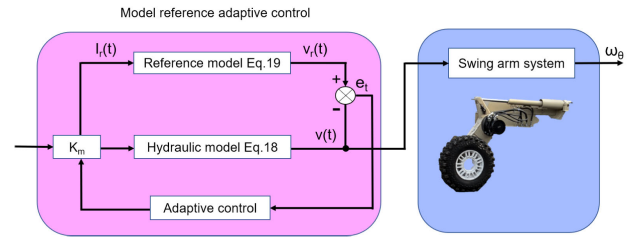


FIGURE 6. Control block diagram of MRAC.

The reference model is chosen as:

$$v_r(s) = K_{fr} K_{vr} I(s)/s_1 (1 + b_T s) \quad (30)$$

From the analysis of the kinematic model of swing arms, the relations of the velocity of the hydraulic cylinder v_p and angular velocity of swing arms w_θ can be expressed as:

$$w_\theta = -2L_C v_p \sin(\mu + \sigma + \theta)/2L_{CB} L_A \quad (31)$$

The main object of the adaptive control is to design a control law K_m based on local parameter optimization to minimize the performance of \hat{J}

$$\hat{J} = \int_0^\infty e^2(\tau) d\tau = \hat{J}_{\min} \quad (32)$$

Taking the partial derivative of the Eq.32, and with a certain step α_s according to the gradient descent method, we can obtain:

$$\begin{aligned} \Delta K_m &= -\alpha_s \partial \hat{J} / \partial K_m = -\alpha_s \int_0^\infty 2e \partial e / \partial K_m d\tau \\ \dot{K}_m &= -2\alpha_s e \partial e / \partial K_m \end{aligned} \quad (33)$$

From the control block diagram shown in Fig6, we can obtain:

$$e(s)/I_r(s) = (K_{fr} K_{vr} - K_m K_f K_v) / S_1 (1 + b_T s) \quad (34)$$

Taking the partial derivative of Eq.34, we obtain:

$$\partial e(s) / \partial K_m = -K_f K_v I_r(s) / S_1 (1 + b_T s) \quad (35)$$

Combing Eq.35 with Eq.30, the result is:

$$\partial e(s) / \partial K = -K_f K_v v_r(s) / K_{fr} K_{vr} \quad (36)$$

Substituting Eq.36 into Eq.23, the adaptive control law based on parameter k_m is obtained as follows:

$$\dot{K}_m = 2\alpha e(s) K_f K_v v_r(s) / K_{fr} K_{vr} \quad (37)$$

Applying the model reference adaptive controller, the velocity of the hydraulic cylinder v can track the model reference output v_r , which guarantees the tracking performance of angular velocity w_θ by minimizing the performance of \hat{J} during the obstacle surmounting. Moreover, the feedback information is estimated by applying the Kalman filter [31].

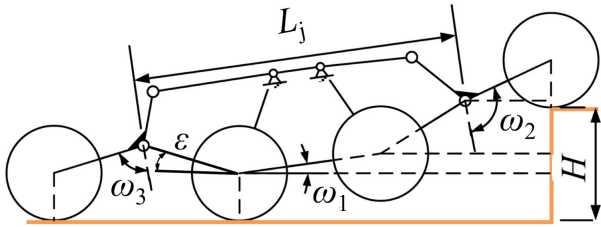


FIGURE 7. Motion planning process of the ATV.

IV. OBSTACLE SURMOUNTING STRATEGY

A. POSTURE PLANNING STRATEGY FOR THE SWING ARMS

Applying the model reference adaptive controller, the velocity of the hydraulic cylinder v can track the model reference output v_r , which guarantees the tracking performance of angular velocity w_θ by minimizing the performance of \dot{J} during the obstacle surmounting.

A constraint function is established to obtain the optimal posture for the swing arm:

$$\begin{aligned} \cos(\omega_2 + \omega_1) &= \frac{L_m \sin \omega_1 + L_f \sin(\omega_1 + \epsilon) - H}{L_{AB}} \\ \cos(\omega_3 - \omega_1) &= \frac{2H - (L_m + L_j) \sin \omega_1 + L_f \sin(\omega_1 + \epsilon)}{L_{AB}} \end{aligned} \quad (38)$$

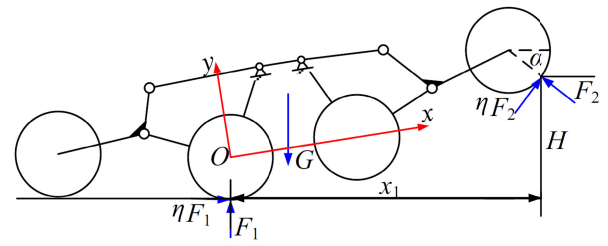
Based on Eq.8, the relation between the radian angles of swing arms and the obstacle height is obtained. The ω_2 is set as the maximum angle (110°) in the initial state of the obstacle surmounting, which provides the maximum ability of the ATV to climb the obstacle. Moreover, the rear swing arm should follow the constraint function in Eq.38 while the ATV drives the swing arms to the minimum angles, $\omega_2 = \omega_3 = 30^\circ$.

B. OBSTACLE SURMOUNTING

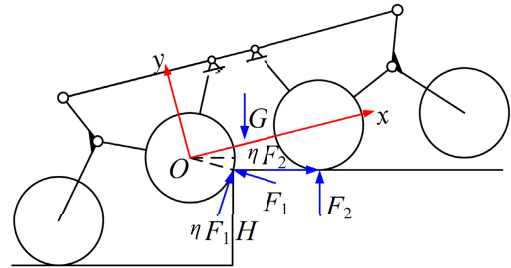
The critical issue of kinematics for the ATV to surmount obstacles is to realize the attitude planning through the actions of the swing arms. An optimized motion attitude planning is of great significance for the autonomous obstacle surmounting control of the ATV. In the kinematics analysis, the ATV achieves obstacle surmounting mainly through motions of the front swing arm, the rear swing arm and the wheels. Therefore, in order to obtain the optimal motion posture of the obstacle surmounting, the three motion will be analyzed in combination to guarantee efficient obstacle surmounting.

During the front wheel climbing process, the rear wheels are off the ground, which can not provide the driving force. Fig.8(a) shows the quasi-static surmounting model of the front wheels. In the surmounting process, the dynamic expression of ATV can be expressed:

$$\begin{cases} F_1 \eta + F_2 (\eta \sin \alpha - \cos \alpha) = 0 \\ F_1 + F_2 (\eta \cos \alpha + \sin \alpha) - G = 0 \\ F_2 [x_1 (\eta \cos \alpha + \sin \alpha) + (H - R) (\cos \alpha - \eta \sin \alpha)] \\ + F_1 \eta R - G (x_g \cos \theta - y_g \sin \theta) = 0 \end{cases} \quad (39)$$



(a) The front wheels



(b) The middle wheels

FIGURE 8. Surmounting obstacle process of the all terrain vehicle.

where (x_g, y_g) is the center of gravity of the ATV, x_1 is the distance between the middle wheel of the main body and the obstacle obtained from the geometric analysis:

$$\begin{aligned} R \sin \alpha &= R + L_m \sin \theta + L_f \sin(\theta + \epsilon) \\ &\quad - L_{AB} \cos(\theta + \omega_2) - H \\ x_1 &= L_m \cos \theta + L_f \cos(\theta + \epsilon) \\ &\quad + L_{AB} \sin(\theta + \omega_2) + R \cos \alpha \end{aligned} \quad (40)$$

The maximum driving force $\eta F_i (i=1,2)$ of the ATV is limited by the adhesion coefficient. In the case of a small adhesion coefficient, the ATV cannot have enough driving force, which will result in a wheel slipping during the obstacle surmounting. According to the theory of ground vehicles, the conditions for determining the ATV not to slip is defined as:

$$\eta F_i \leq F_i \tan \lambda \quad (41)$$

where λ denotes the internal friction angle of the soil, in the experiment $\lambda = 35^\circ$. Combining Eq.39 with Eq.41, the constraint height H is obtained as:

$$H(\omega_1, \psi) \leq H \leq H(\omega_1) \quad (42)$$

where $H(\omega_1, \psi)$ denotes the function of ground attachment, $H(\omega_1)$ denotes the function of the planning constraint, and ψ denotes the attachment coefficient value, in the experiment $\psi = 0.5$. The obstacle surmounting constraint curve obtained through analysis is shown in Figure9. The red area in the figure is the feasible region of the obstacle surmounting height and the angle of the front swing arms.

Fig.8(b) shows the surmounting process of the middle wheels. When the front and rear swing arm get the lowest position, the ATV has the maximum surmounting ability.

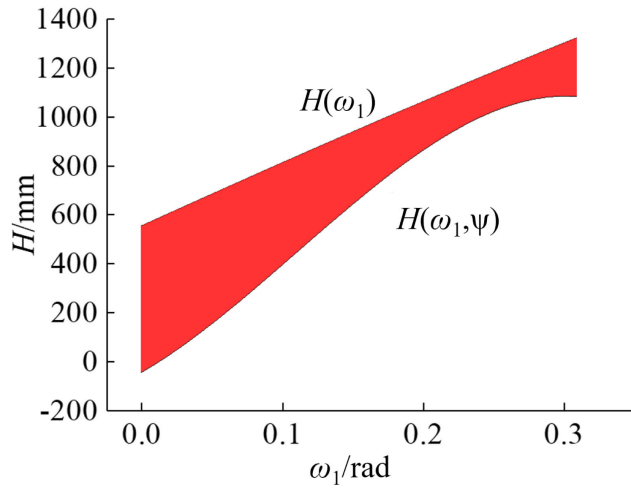


FIGURE 9. Constraint of the front wheel surmounting.

And the contact force of the rear wheels is zero since of the off-road state of the rear wheels.

$$\begin{cases} F_1(\varphi \sin \alpha - \cos \alpha) + F_2\varphi = 0 \\ F_1(\varphi \cos \alpha + \sin \alpha) + F_2 - G = 0 \\ F_1\varphi R + F_2(\varphi R \sin \alpha + L_m \cos \alpha) \\ - G(x_g \cos \theta - y_g \sin \theta) = 0 \end{cases} \quad (43)$$

$$\begin{cases} N_{m1}(\varphi \sin \alpha - \cos \alpha) + N_{m2}\varphi = 0 \\ N_{m1}(\varphi \cos \alpha + \sin \alpha) + N_{m2} - G = 0 \\ N_{m1}\varphi R + N_{m2}(L_m \cos \omega_1 + \varphi R \sin \alpha) \\ - GR \cos \alpha = 0 \end{cases} \quad (44)$$

According to the geometric relationship, we can get

$$\sin \alpha = 1 + \frac{L_{AB} \cos(\omega_3 - \theta) - L_f \sin(\epsilon - \theta) - H}{R} \quad (45)$$

Combing Eq.41, Eq.44 and Eq.45, The geometric constraint function of the center of mass is defined as:

$$H = R - x_g \sin \theta - y_g \cos \theta + 3L_{AB} \cos(\omega_3 - \theta) - 3L_f \sin(\epsilon - \theta) \quad (46)$$

The obstacle surmounting the constraint curve of the middle wheels is shown in Figure 10. The red area in the figure is the feasible region of the obstacle surmounting height and the angle of front swing arms.

From the analysis above, the maximum height value of the obstacle from the obstacle surmounting curve Fig. 10 is obtained as $H = 957mm$. Moreover, substituting the maximum height in the Eq.43 and Eq.46 the required driving torque for obstacle surmounting is $2830.2N \cdot m$. Furthermore, the initial planning of the obstacle process is shown in Fig. 11. In Fig. 11 (a), the ATV is in the initial state of eight-wheel driving. When the obstacle is detected, the swing arms change to the initial posture for obstacle surmounting. And the swing angles of the front and rear swing arms are planned according

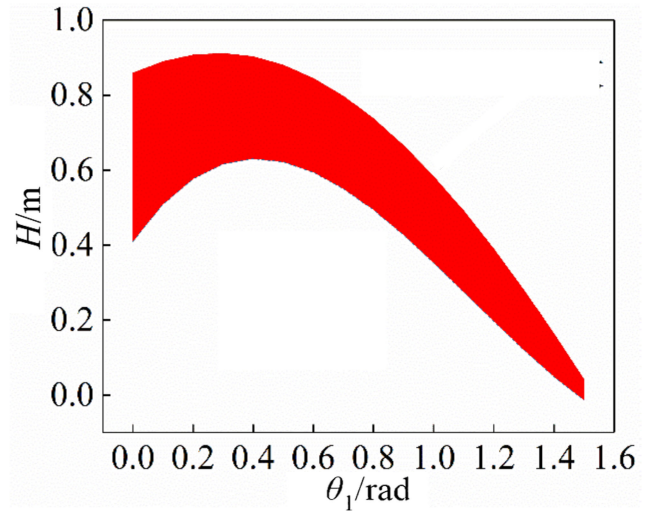


FIGURE 10. Constraint of the middle wheel surmounting.

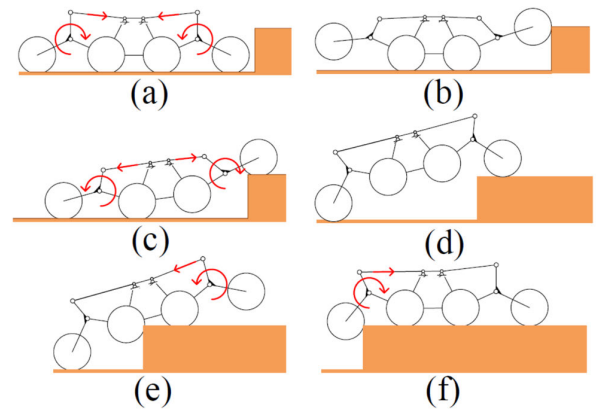


FIGURE 11. Surmounting process of the all terrain vehicle.

to the height information. Fig. 11 (b)-(c) is the adaptation process of the ATV and the ground. Through this process, the front wheels have contact with the obstacle. Fig. 11 (d) is the obstacle climbing stage of the front wheel, while Fig. 11 (e) is the obstacle climbing stage of the middle wheel. The front and rear swing arms are retracting down to increase the position of the center of mass of the ATV, after the front wheel surmounts the obstacle successfully. In order to guarantee the stability of the center of mass, the front swing arm is gradually restored to the initial position. In Fig. 11 (f), the swing arm reaches the initial position while the obstacle surmounting process is completed.

C. STABILITY ANALYSIS

In the obstacle surmounting, the center of mass will change according to the irregular terrain and skidding is inevitable in the process. Therefore, it is necessary to analyze the stability to avoid tipping over during the obstacle surmounting. The stability of the vehicle refers to the ability of the platform to dynamically adjust itself to resist instability after a sudden

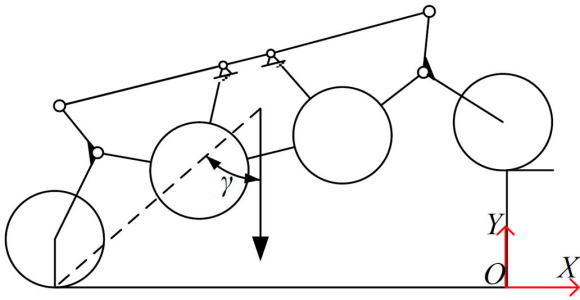


FIGURE 12. Stability analysis of the all terrain vehicle.

change (instantaneous speed, acceleration or abnormal forces on the ground) in its motion state. The stability of the ATV is analyzed by applying the centroid projection method. When the centroid projection of the ATV falls in the polygonal projection area of the unmanned platform on the ground, it is considered in a stable state; otherwise it will tip over or rollover due to instability.

The obstacle surmounting stability of the ATV is judged from the stability margin, and the centroid projection method is used for analysis. From Fig.11, it can be seen that Fig.11 (d) is the most dangerous state in the obstacles surmounting. Therefore, the stability analysis of the process (d) is analyzed as Eq.47.

$$\tan \gamma = \frac{{}^0C_x}{{}^0C_y} \quad (47)$$

Combing Eq.19 and Eq.47, the stability margin angle of the ATV is defined as:

$$\gamma = \arctan \frac{Ac_1 - Bs_1 + Md_x}{As_1 + Bc_1 + Md_y} \quad (48)$$

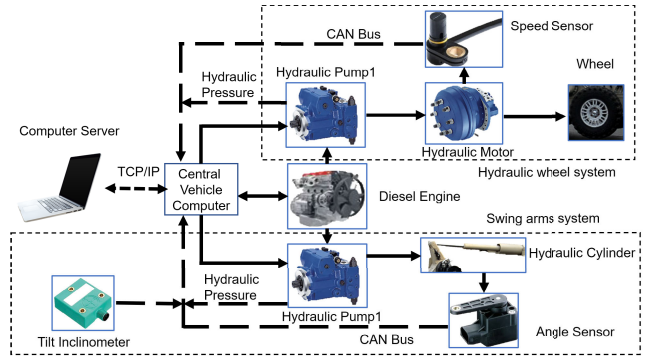
Therefore, the stability of the ATV is related to the pitch angle and the front and rear swing arm angles. In the obstacle surmounting, the attitude of the ATV should be controlled to ensure the stability of the ATV.

V. SURMOUNTING EXPERIMENT

A. THE ALL TERRAIN VEHICLE PLATFORM

The control system of the ATV (Dragon horse, Sunward Intelligent Equipment Co., Ltd, China) is composed of a central vehicle computer, a ground-station computer server, a hydraulic driving system, and a swing arms system, as shown in Fig.13.

The computer server is utilized for motion planning and control. The central vehicle computer (DSC56800E, Freescale, USA) is applied for real-time electro-hydraulic control and sensor signal acquisition. The hydraulic pressure sensors, speed sensors, tilt inclinometer and angle sensor communicate with the central vehicle computer by CAN protocol(CAN bus, <https://www.canbus.us/>). The communications between the ground-station computer server and the central vehicle computer are carried out using the wireless TCP-IP protocol.



(a) Structure of the platform



(b) All terrain vehicle Dragon Horse

FIGURE 13. All terrain vehicle platform.

TABLE 3. The parameters of the ATV.

Parameter	Name	Value
m_1	weight of the main body(kg)	2800
m_2	weight of the front swing arm(kg)	200
m_3	weight of the rear swing arm(kg)	200
T	wheel motor torque(Nm)	4,047
L_m	intermediate wheelbase(mm)	1000
L_f	bevel chassis length(mm)	1000
L_j	the ATV length(mm)	2900
R	radius of the wheel(mm)	417.5
ϵ	chassis approach angle(degree)	18

The torque of hydraulic motor T_m is calculated as:

$$T_m = \frac{1}{2\pi} \Delta p_h V_h \quad (49)$$

where Δp_h is the pressure difference between inlet and outlet of hydraulic motor, V_h is hydraulic motor displacement.

B. EXPERIMENT

In order to verify the kinematic and obstacle surmounting performance of the ATV, the surmounting simulation is utilized by applying Automatic Dynamic Analysis of Mechanical Systems (ADAMS) and SolidWorks. The 3D model of the ATV is established in the Solidworks then imported to ADAMS. The simulation process of the obstacle surmounting is shown in Fig.14. According to Eq.4, angle-based attitude planning is transformed into attitude planning based on hydraulic cylinder stroke. The Trace of the gravity center of mass is shown in Fig.15, which verifies the analysis of the gravity center. The simulation verified that the ATV could climb a vertical wall up to 950mm height.

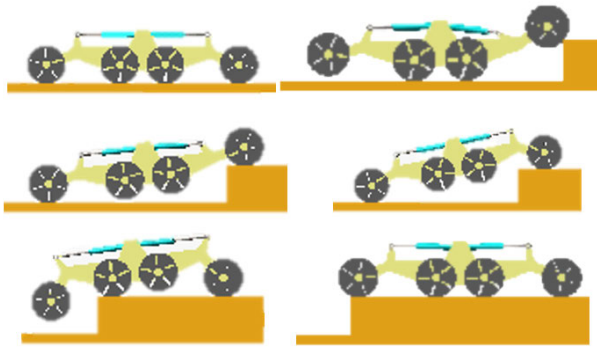


FIGURE 14. Simulation of the all terrain vehicle obstacle surmounting.

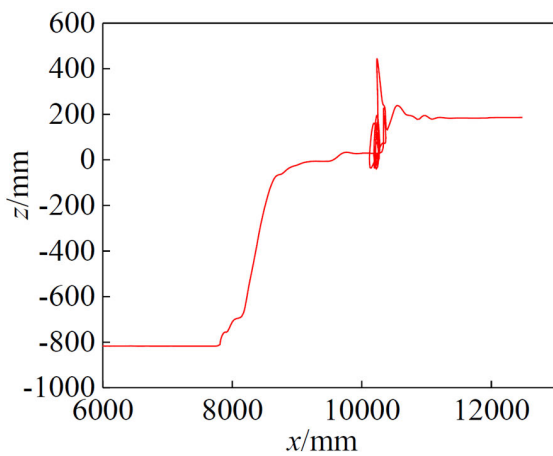


FIGURE 15. The trace of the gravity center of mass in the simulation.

The obstacle surmounting experiment is carried out on the vertical concrete wall in the mountain, and the obstacle surmounting process verifies the simulation, as shown in Fig.16. The experiment results show that the ATV can surmount a 950mm height obstacle. The posture planned in the simulation and experiment is shown in Fig.17. When the ATV detected the obstacle, hydraulic swing arms changes to the initial posture for obstacle surmounting at 1.3s. In the front swing arm surmounting process(3-6s), there was an instantaneous change in 4s after the swing arm moved to the maximum angle when the front swing arms contacted the vertical wall directly. After the rear swing arm surmounting process(6-7s), the ATV has surmounted the obstacle successfully. It can be seen from the power output of the experiment, shown in Fig.18, the hydraulic pump power is lower than the engine power during the climbing process, indicating that the system is operating stably. And the torque output of the experiment is shown in Fig.19. The maximum torques of experiment and simulation are 2618 N·m and 2657 N·m, respectively. The maximum output torque of the hydraulic motor occurs in the two key stages of the front wheel obstacle surmounting (Fig. 16b) and the middle wheel obstacle surmounting (Fig. 16e). The adhesion and collision force are

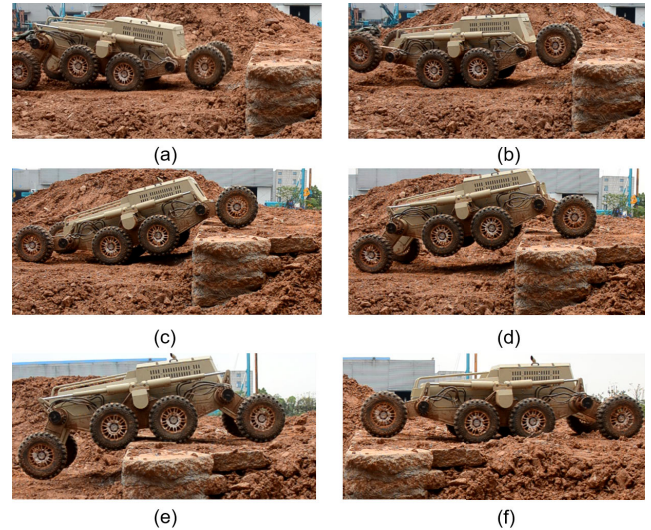


FIGURE 16. Experiment of the all terrain vehicle obstacle surmounting.

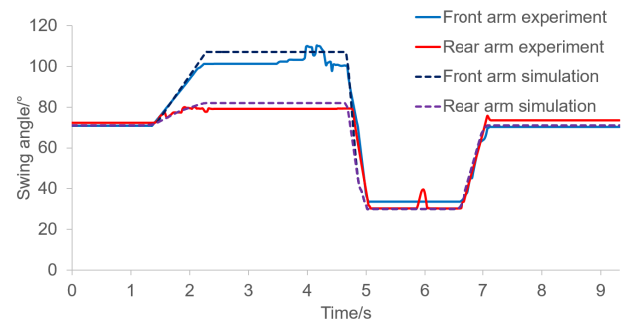


FIGURE 17. Posture control results of simulations and experiments.

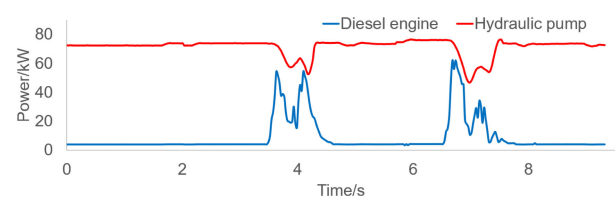


FIGURE 18. Power output of the experiment.

greater in the two stages, and the maximum output torque is less than the rated torque of hydraulic motor, which verifies the feasibility of obstacle surmounting.

Because the hydraulic mechanism in the simulation model is an ideal constraint, the posture planning process in the simulation is relatively smooth. Moreover, the effect of the environmental damping spring is not considered. Therefore, the curve is a typical step curve. In the front swing arm obstacle surmounting, there was a instantaneous sudden change in the 4s after the swing arm reaches the maximum angle, and the instantaneous angle was about 10°. When the ATV collides

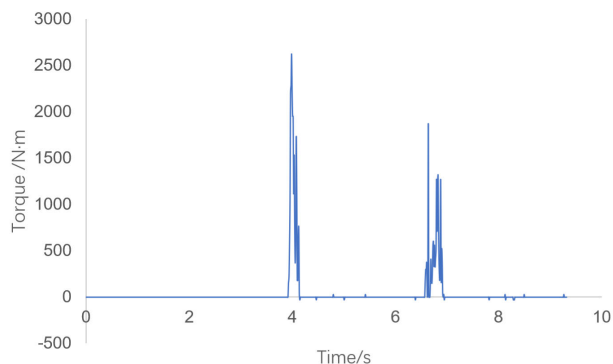


FIGURE 19. Torque output of the experiment.



FIGURE 20. Terrain adaptive of the all terrain vehicle.

with the vertical wall, the damping spring acts and triggers the swing angle instantaneous fluctuations, which verifies the reliability of the vehicle design and cushion hydraulic cylinder.

Although the obstacle surmounting process is highly dynamical, the posture control curves show that the experiment results well agree with the simulation ones, which verify that the motion control method is efficient. Finally, the terrain adaptive experiment is utilized as shown in Fig. 20.

VI. CONCLUSION AND FUTURE WORK

Existing bionic mechanisms such as quadruped-legged robots, inchworm-like robots, gecko-like adhesion robots, as well as planetary vehicle rocker with arm suspension are all geared towards miniature and lightweight mobility. Those robots have poor load capacity and require complex control strategies, which cannot meet the engineering requirements for platform transportability and maneuverability under battlefield conditions.

To meet the requirement of the ATV on unstructured terrain and improve the robot vehicle adaptive ability, we propose a novel horse inspired ATV “Dragon Horse”, driven by distributed hydraulic motors. The horse inspired concept and kinematic model of the ATV are studied to enhance the stability of the ATV. Afterward, the hydraulic model and posture control method based on MRAC are proposed in this article. Moreover, the dynamic performance of ATV in the obstacle

surmounting is analyzed. Additionally, the simulation is executed in Adams to verify the analysis and strategy. Finally, the experiment is demonstrated for climbing a vertical wall, which is a typical terrain in the mountain battlefield. The dynamic performance of ATV and wheel dynamics coupling effects will be considered in the future, which includes the non-linear dynamic effects and deformation of the wheel with the ground. In the future, we will focus on improving the environmental perception and high-level autonomous ability of the ATV applying the Lidar sensor and camera to achieve fully automatic obstacle surmounting. For example, applying camera sensors to detect the environment and analyze the boundaries of feasible roads to provide path planning in the mountain battlefield.

REFERENCES

- [1] J. Peterson, W. Li, B. Cesar-Tondreau, J. Bird, K. Kochersberger, W. Czaja, and M. McLean, “Experiments in unmanned aerial vehicle/unmanned ground vehicle radiation search,” *J. Field Robot.*, vol. 36, no. 4, pp. 818–845, Jun. 2019.
- [2] Y. Liu, Z. Luo, Z. Liu, J. Shi, and G. Cheng, “Cooperative routing problem for ground vehicle and unmanned aerial vehicle: The application on intelligence, surveillance, and reconnaissance missions,” *IEEE Access*, vol. 7, pp. 63504–63518, 2019.
- [3] M. Hutchinson, C. Liu, and W. Chen, “Source term estimation of a hazardous airborne release using an unmanned aerial vehicle,” *J. Field Robot.*, vol. 36, no. 4, pp. 797–817, Jun. 2019.
- [4] J. Zhang, Z. Yu, S. Mao, S. C. G. Periaswamy, J. Patton, and X. Xia, “IADRL: Imitation augmented deep reinforcement learning enabled UGV-UAV coalition for tasking in complex environments,” *IEEE Access*, vol. 8, pp. 102335–102347, 2020.
- [5] J. Farrant and C. M. Ford, “Autonomous weapons and weapon reviews: The UK second international weapon review forum,” *Int. Law Stud.*, vol. 93, no. 1, p. 13, 2017.
- [6] Y. Zhu, Y. Fei, and H. Xu, “Stability analysis of a Wheel-Track-Leg hybrid mobile robot,” *J. Intell. Robot. Syst.*, vol. 91, nos. 3–4, pp. 515–528, Sep. 2018.
- [7] J. Gwozdz, “Enabling semi-autonomous manipulation on Irobot’s Packbot,” Ph.D. dissertation, Worcester Polytech. Inst., Worcester, MA, USA, 2014.
- [8] X. Zhou, X. Yu, Y. Zhang, Y. Luo, and X. Peng, “Trajectory planning and tracking strategy applied to an unmanned ground vehicle in the presence of obstacles,” *IEEE Trans. Autom. Sci. Eng.*, early access, Aug. 4, 2020, doi: 10.1109/TASE.2020.3010887.
- [9] S.-H. Hyon, Y. Ida, J. Ishikawa, and M. Hiraoka, “Whole-body locomotion and posture control on a torque-controlled hydraulic rover,” *IEEE Robot. Autom. Lett.*, vol. 4, no. 4, pp. 4587–4594, Oct. 2019.
- [10] D. Wooden, M. Malchano, K. Blankespoor, A. Howardy, A. A. Rizzi, and M. Raibert, “Autonomous navigation for BigDog,” in *Proc. IEEE Int. Conf. Robot. Autom.*, May 2010, pp. 4736–4741.
- [11] S. Kuindersma, R. Deits, M. Fallon, A. Valenzuela, H. Dai, F. Permenter, T. Koolen, P. Marion, and R. Tedrake, “Optimization-based locomotion planning, estimation, and control design for the atlas humanoid robot,” *Auto. Robots*, vol. 40, no. 3, pp. 429–455, Mar. 2016.
- [12] Z. B. Rivera, M. C. De Simone, and D. Guida, “Unmanned ground vehicle modelling in Gazebo/ROS-based environments,” *Machines*, vol. 7, no. 2, p. 42, Jun. 2019.
- [13] A. J. Clark, K. A. Cissell, and J. M. Moore, “Evolving controllers for a transformable wheel mobile robot,” *Complexity*, vol. 2018, pp. 1–12, Dec. 2018.
- [14] J. M. García, J. L. Martínez, A. Mandow, and A. García-Cerezo, “Caster-leg aided maneuver for negotiating surface discontinuities with a wheeled skid-steer mobile robot,” *Robot. Auto. Syst.*, vol. 91, pp. 25–37, May 2017.
- [15] W.-H. Chen, H.-S. Lin, Y.-M. Lin, and P.-C. Lin, “TurboQuad: A novel Leg-Wheel transformable robot with smooth and fast behavioral transitions,” *IEEE Trans. Robot.*, vol. 33, no. 5, pp. 1025–1040, Oct. 2017.
- [16] Y. Zhang, L. Zhang, W. Wang, Y. Li, and Q. Zhang, “Design and implementation of a two-wheel and hopping robot with a linkage mechanism,” *IEEE Access*, vol. 6, pp. 42422–42430, 2018.

- [17] M. He, J. He, and S. Scherer, "Model-based real-time robust controller for a small helicopter," *Mech. Syst. Signal Process.*, vol. 146, Jan. 2021, Art. no. 107022.
- [18] H. Miura, A. Watanabe, M. Okugawa, T. Miura, and T. Koganeya, "Plant inspection by using a ground vehicle and an aerial robot: Lessons learned from plant disaster prevention challenge in world robot summit 2018," *Adv. Robot.*, vol. 34, no. 2, pp. 104–118, Jan. 2020.
- [19] A. Jacobson, F. Zeng, D. Smith, N. Boswell, T. Peynot, and M. Milford, "What localizes beneath: A metric multisensor localization and mapping system for autonomous underground mining vehicles," *J. Field Robot.*, Aug. 2020, doi: [10.1007/s12555-019-0927-2](https://doi.org/10.1007/s12555-019-0927-2).
- [20] M. H. Jilin He, "Robust flight control of a small unmanned helicopter," *Robot.*, vol. 38, nos. 337–342 and 351, 2016.
- [21] J. Li, J. Wang, H. Peng, L. Zhang, Y. Hu, and H. Su, "Neural fuzzy approximation enhanced autonomous tracking control of the wheel-legged robot under uncertain physical interaction," *Neurocomputing*, vol. 410, pp. 342–353, Oct. 2020.
- [22] J. Li, J. Wang, S. Wang, W. Qi, L. Zhang, Y. Hu, and H. Su, "Neural approximation-based model predictive tracking control of non-holonomic wheel-legged robots," *Int. J. Control, Autom. Syst.*, pp. 1–10, Sep. 2020, doi: [10.1002/rob.21978](https://doi.org/10.1002/rob.21978).
- [23] B. Torossian, F. Bekkers, T. Sweijts, M. Roelen, A. Hristov, and S. Atalla, *The Military Applicability of Robotic and Autonomous Systems*. Hague, The Netherlands: Hague Centre for Strategic Studies, 2020.
- [24] G. Taylor, M. Quist, M. Lanting, C. Dunham, and P. Muench, "Multi-modal interaction for robotics mules," in *Proc. 21st Unmanned Syst. Technol., Int. Soc. Opt. Photon.*, vol. 10195, May 2017, Art. no. 101950T.
- [25] S. Ding, L. Liu, and W. X. Zheng, "Sliding mode direct yaw-moment control design for in-wheel electric vehicles," *IEEE Trans. Ind. Electron.*, vol. 64, no. 8, pp. 6752–6762, Aug. 2017.
- [26] S. Ding, L. Liu, and J. H. Park, "A novel adaptive nonsingular terminal sliding mode controller design and its application to active front steering system," *Int. J. Robust Nonlinear Control*, vol. 29, no. 12, Jun. 2019.
- [27] S. Fahmi, C. Mastalli, M. Focchi, and C. Semini, "Passive whole-body control for quadruped robots: Experimental validation over challenging terrain," *IEEE Robot. Autom. Lett.*, vol. 4, no. 3, pp. 2553–2560, Jul. 2019.
- [28] E. Koco, A. Mutka, and Z. Kovacic, "New variable passive-compliant element design for quadruped adaptation to stiffness-varying terrain," *Int. J. Adv. Robotic Syst.*, vol. 13, no. 3, p. 90, Jun. 2016.
- [29] R. Galati and G. Reina, "Terrain awareness using a tracked skid-steering vehicle with passive independent suspensions," *Frontiers Robot. AI*, vol. 6, p. 46, Jun. 2019.
- [30] M. He, C. Ren, J. He, K. Wu, Y. Zhao, Z. Wang, and C. Wu, "Design, analysis and experiment of an eight-wheel robotic vehicle with four-swing arms," *Ind. Robot, Int. J. Robot. Res. Appl.*, vol. 46, no. 5, pp. 682–691, Aug. 2019.
- [31] M. He and J. He, "A dynamic enhanced robust cubature Kalman filter for the state estimation of an unmanned autonomous helicopter," *IEEE Access*, vol. 7, pp. 148531–148540, 2019.



JILIN HE received the Ph.D. degree in mechatronic engineering from Shanghai Jiaotong University, China, in 2004. He is currently an Associate Professor and the Ph.D. Mentor with the College of Mechanical and Electrical Engineering, Central South University. His current research interests include mechatronics and robotics



QINGHUA HE is currently a Full Professor with the Central South University, Changsha, China. He is the Head of the Department of Engineering Equipment Design and Control. He is the Founder and the Chairman of the Sunward Intelligent Equipment Company Ltd., since 1999. He is the Director of the Intelligent Robot Committee of the Chinese Society of Artificial Intelligence and the Director of the Chinese Society of Construction Machinery.



CHANGJI REN received the master's degree from the College of Mechanical and Electrical Engineering, Central South University, China, in 2019. His research interests include mechanical design and motion control of unmanned vehicles.



BHUSHAN received the bachelor's degree in automation and robotics engineering from Visvesvaraya Technological University, Karnataka, India. He is currently pursuing the master's degree in control engineering, Sapienza University of Rome, Italy. He is working on his thesis at the Neuroengineering and Medical Robotics Laboratory (NEARLab), Department of Electronics, Information and Bioengineering (DEIB), Politecnico di Milano, Italy. His research interests include passivity-based control and its application in robot-assisted minimally invasive surgery.



MIAOLEI HE (Member, IEEE) received the Ph.D. degree from the College of Mechanical and Electrical Engineering, Central South University, China, in 2019. He is currently a Lecturer with the College of Engineering and Design, Hunan Normal University, China. He was a Visiting Scholar with the Robotics Institute, Carnegie Mellon University. His research interests include robot motion control and motion planning.



XUANYI ZHOU (Graduate Student Member, IEEE) received the bachelor's degree from Hunan University, Changsha, China. He is currently pursuing the Ph.D. degree with Central South University. He is also working on research projects with the Neuroengineering and Medical Robotics Laboratory (NEARLab) and the Department of Electronics, Information and Bioengineering (DEIB), Politecnico di Milano. His research interests include intelligent control and its application in hydraulic robot.